Infrared Spectra of Rhodium Hydrides in Solid Argon, Neon, and Deuterium with Supporting Density Functional Calculations

Xuefeng Wang and Lester Andrews*

Department of Chemistry, University of Virginia, Charlottesville, Virginia 22904-4319

Received: September 26, 2001; In Final Form: January 7, 2002

Laser-ablated Rh atoms react with H_2 to give RhH_2 and RhH as primary products, which are trapped or react with additional hydrogen in the condensing solid argon, neon, and deuterium matrixes. RhH gives a major 1920.6 cm^{-1} band in argon, a minor 1935.5 cm^{-1} band in neon, and no absorption in deuterium. RhH_2 produces sharp 2099.4 and 2053.4 cm^{-1} and 2099.7 and 2052.2 cm^{-1} bands in solid argon and neon, respectively and no absorption in deuterium; these absorptions increase on annealing the matrix to allow diffusion, which shows that ground state Rh inserts spontaneously into H_2. Additional absorptions at 2122.4 and 2078.2 cm^{-1} (1527.3 and 1494.4 cm^{-1} with D_2) in neon and at 1521.1 and 1496.1 cm^{-1} in deuterium are assigned to the higher hydride complexes $(H_2)RhH_3$ and $(H_2)RhH_2$, respectively. A weaker 737.6 cm^{-1} absorption in neon is due to the side-bound complex $Rh(H_2)_2$. Both $(D_2)RhH_2$ and $Rh(H_2)(D_2)$ rearrange H and D on photoexcitation suggesting a tetrahedral transition state. Rhombic $(RhH)_2$ is observed in all three matrix systems. These assignments are supported by D_2, HD, and $H_2 + D_2$ substitution and density functional theory frequency and structure calculations.

Introduction

Rhodium is one of the most important metals in catalysis. Rhodium-supported catalyst systems are used for many important reactions including the hydrogenation of carbon monoxide.[1] In particular, rhodium in the supported unsaturated Rh(CO) intermediate can activate dihydrogen.[2] Thus, it is fundamental to understand the reactivity of a naked Rh atom with H_2. Theoretical calculations have suggested that ground-state Rh(^{4}F) has to surmount a large energy barrier for insertion to give the ground state ($^2A_1$) RhH_2 dihydride but that excited (^{2}F) state Rh can insert spontaneously into the dihydrogen bond.[3] The RhH_2 molecule formed in the hydrogen reaction has been characterized by ESR spectroscopy in solid argon and krypton.[4] This is analogous to our finding that Pt inserts into hydrogen to give PtH_2, but in contrast, Pd forms the side-bonded complex $Pd(H_2)$.[5,6]

Electronic spectra of RhH and RhD have been characterized recently using a molecular beam laser vaporization source.[7] Several earlier theoretical calculations[8−11] predict the $^3\Delta$ ground state for RhH, which is confirmed by experiment.[7] A weakly bound Rh−H species on Rh/Al_2O_3 absorbing at 2013 cm^{-1} is important for reactions involving H_2 over supported rhodium.[12,13] The Rh−H stretching mode for organometallic rhodium hydride complexes generally falls in the 2000−2150 cm^{-1} range.[14−16] Furthermore, rhodium monohydride $HRh(I)L_4$ complexes are important hydride transfer agents in synthetic chemistry.[17,18]

Higher hydrides have been characterized for the group 4 and 5 transition metals in matrix isolation experiments.[19−23] One question for rhodium hydride is the bonding mode for a second H_2 molecule: will it be side-bonded as in $Pd(H_2)_2$, a tetrahydride as in ZrH_4, or a mixture of both types? Calculations have characterized a pyramidal structure for RhH_3 in the ground state[11] and a higher side-bonded $(H_2)RhH_3$ hydride species.[24] Here follows a combined matrix infrared spectroscopic and density functional theoretical investigation of rhodium hydrides, which characterizes the simple rhodium hydrides RhH and RhH_2 and provides considerable evidence for their higher complexes with dihydrogen.

* To whom correspondence should be addressed. E-mail: lsa@virginia.edu.

Experimental and Theoretical Methods

The experimental methods and apparatus employed for Rh atom reactions have been described in previous publications.[25−28] Matrix-isolation experiments were performed for Rh atoms and H_2 in excess argon frozen on 7 and 4 K substrates and excess neon and deuterium on a 4 K cesium iodide window. Infrared spectra were recorded, samples were annealed and irradiated, and more spectra were recorded.

DFT calculations were performed using the Gaussian 98 program system;[29] B3LYP and BPW91 density functionals;[30,31] 6-311+G(d,p), 6-311++G(d,p), and 6-311+G(3df, 3pd) for H;[32] and LANL2DZ and SDD pseudopotentials (18 valence electron) for Rh.[33,34] Geometries were fully optimized, and the vibrational frequencies were computed analytically from second derivatives.

Results

Infrared spectra of products formed in the reaction of laser-ablated rhodium and dihydrogen in excess argon and neon, and in pure deuterium, during condensation at 7 and at 4 K will be presented in turn. Density functional calculations were performed on rhodium hydrides to support their identification through matrix infrared spectroscopy.

Argon. Infrared spectra in the Rh-H and Rh-D stretching regions are shown in Figures 1−3 for the Rh reaction with 2% H_2, D_2, and HD in excess argon. For H_2, strong bands were observed at 1920.6 and 2053.4 cm^{-1}, and the latter was reduced to one-half by full arc photolysis but restored on annealing to 30 K. A new very weak band was found at 2099.4 cm^{-1}. Other features at 2036.1, 2014.0, and 1980 cm^{-1} are relatively stronger

10.1021/jp013624f CCC: $22.00
Published on Web 03/19/2002

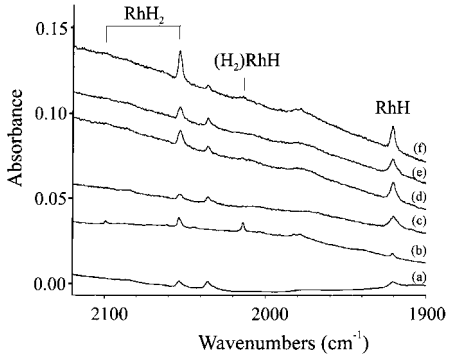

Figure 1. Infrared spectra of laser-ablated rhodium and hydrogen reaction products in solid argon: (a) 6% H_2 in argon co-deposited at 4 K for 60 min, (b) after annealing to 25 K, (c) 2% H_2 in argon co-deposited at 7 K for 60 min, (d) after annealing to 20 K, (e) after broadband photolysis, and (f) after annealing to 30 K.

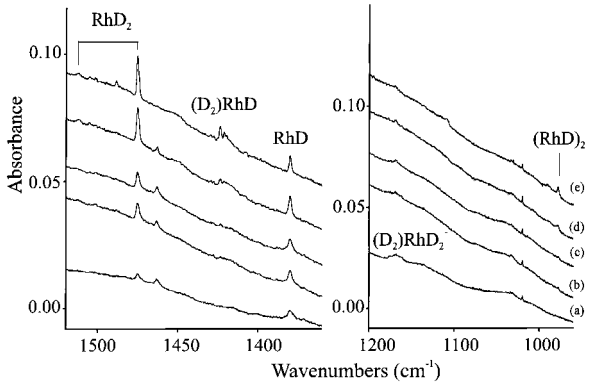

Figure 2. Infrared spectra of laser-ablated rhodium and deuterium reaction products in solid argon: (a) 2% D_2 in argon co-deposited at 7 K for 60 min, (b) after annealing to 20 K, (c) after broadband photolysis, (d) after annealing to 30 K, and (e) after annealing to 35 K.

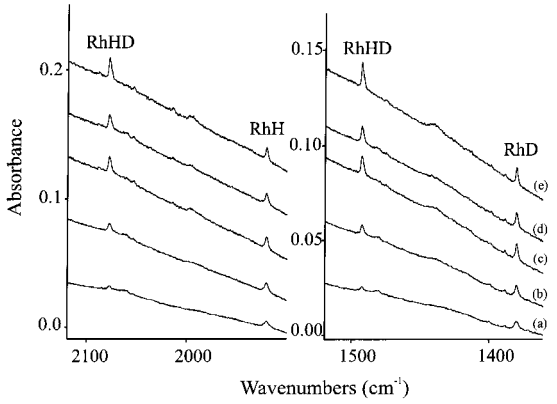

Figure 3. Infrared spectra of laser-ablated rhodium and deuterium hydride reaction products in solid argon: (a) 2% HD in argon co-deposited at 7 K for 60 min, (b) after annealing to 20 K, (c) after broadband photolysis, (d) after annealing to 30 K, and (e) after annealing to 35 K.

with 6% H_2. Deuterium counterparts appeared at 1379.9, 1475.2, and 1512.2 cm^{-1}, respectively. The 1475.2 cm^{-1} band was effected little by ultraviolet radiation but doubled on 30 K annealing. Experiments with H_2 and D_2 together gave the same major product bands. The HD experiment gave the same 1920.6 and 1379.9 cm^{-1} bands but different 2077.9 and 1492.9 cm^{-1} features as shown in Figure 3. The latter features increased 2-fold on 30 K annealing, decreased 15% on UV irradiation, and increased 40% on 35 K annealing. The Ar_nH^+ and Ar_nD^+ species were observed in all of these experiments.[35]

An additional broad 1980 cm^{-1} band with 1422 cm^{-1} deuterium counterpart increased on annealing. Analogous bands were observed at 1998 and 1441 cm^{-1} with HD. Table 1 lists the observed bands.

Neon. The neon matrix spectra are more complicated as more diffusion of H_2 takes place during condensation of neon. Figure 4 reveals 2078.5, 2023.6, 2009.4, 1974.2, and 1936 cm^{-1} absorptions and a sharp weaker 2052.2 cm^{-1} band in the Rh−H stretching region; the weak 2023.6 cm^{-1} band is due to RhCO from trace CO impurity.[27] Annealing to 7 and 9 K increased all absorptions, but the 2052.2 cm^{-1} band increased four times and acquired a 2099.7 cm^{-1} partner, and sharp 1936.9 and 1935.5 cm^{-1} peaks were resolved. Broadband photolysis decreased all absorptions but most notably the sharp bands. However, these absorptions recovered on subsequent annealing to 11 K. A new 1608 cm^{-1} band decreased on annealing and disappeared on photolysis, and a new 1357.2 cm^{-1} band increased on annealing, decreased on photolysis, and restored on further annealing. The HD spectrum compared in Figure 4 reveals new absorptions at 2085.9, 2076.9, and 1990 cm^{-1} and familiar features at 2023.6 and 1935.5 cm^{-1}. Figure 5 compares analogous spectra in the Rh−D stretching region, and the product absorptions are listed in Table 1.

Spectra from $H_2 + D_2$ mixtures in neon are shown in Figure 6. The sharp features give only pure isotopic absorptions, but new mixed isotopic features are observed at 1987.6, 1968.5, and 1432.9 cm^{-1}. The lower frequency regions are illustrated in Figures 7 and 8, which reveals 1608, 1357.2, and new 737.6 cm^{-1} bands and isotopic counterparts.

Deuterium. Pure deuterium has been employed as a reactive matrix,[5,6,23] and a set of spectra for rhodium are shown in Figure 9. Note that all bands are sharp, and that no significant change occurs on photolysis. The observed frequencies are also given in Table 1.

Calculations. DFT calculations were done for RhH and RhH_2 using two functionals, two basis sets, and two pseudopotentials, and the results for the $^3\Delta$ ground-state RhH and $^2A_1$ ground-state RhH_2 are summarized in Table 2. Several higher hydrides were also computed including RhH_3, $(H_2)RhH$, $Rh(H_2)_2$, $(H_2)RhH_2$, and $(H_2)RhH_3$, and the structures and frequencies are given in Table 3. Calculations for RhH_4 failed to converge, and the energy differences between $Rh(H_2)_2$ and low symmetry forms of $(H_2)RhH_2$ were small enough (2.5 kcal/mol) to suggest that both may be observable. The structures of several relevant species are illustrated in Figure 9. The $(RhH)_2$ dimer gave a rhombus structure, and the $^3B_{1u}$ state was 24−28 kcal/mol lower than ^5A_g and ^1A_g states. The results of calculations for RhH_x^- ($x = 1-4$) anions are also given in Table 4.

Discussion

The argon, neon, and deuterium matrix results provide an interesting contrast for the reaction of rhodium atoms with dihydrogen as the solidification rate of these three materials at 4 K decreases in the above order for these experiments.

RhH and RhH_2. A band at 1920.6 cm^{-1} is observed after initial deposition of Rh and H_2 in argon (Figure 1). With 2% H_2, the intensity of this band doubles on annealing to 20 K but reduces on broadband photolysis, and increases further on 30 K annealing; however, with 6% H_2, the band decreases on annealing to 25 K. The D_2 counterpart at 1379.9 cm^{-1} gives an isotopic ratio of 1.3918. Only these two bands are observed in HD indicating that one hydrogen atom is involved in this vibration. The isotopic doublet and H/D ratio support the

TABLE 1: Infrared Absorptions (cm^{-1}) Observed from Reactions of Rhodium and Dihydrogen in Excess Argon, Neon, and Deuterium

argon			neon			deuterium	
H_2	HD	D_2	H_2	HD	D_2	D_2	identification
2272							$(D_2)RhD_3$
2234							$(D_2)RhD_2$
			2122.4	2093.6[a]	1527.3	1521.1	$(H_2)RhH_3$
2099.4		1512.2	2099.7		1512.0		RhH_2, ν_1
			2078.2	2085.9[a]	1494.4	1496.1	$(H_2)RhH_3$
2053.4	2077.9	1475.2	2052.2	2076.9	1475.0		RhH_2, ν_3
2036.1	2059.8	1463.1	2046.6	2071.2	1471.8		RhH_2 site
	1492.9			1492.5			RhHD
	1480.7			1489.3			RhHD site
2030 (sh)	1463	1469.1					$(H_2)RhH_2^-$
2014.0	2013.5						$(H_2)RhH$
	1427.6	1423.7					$(D_2)RhD$
			2009.4		1448.0	1448.4	$(H_2)RhH_2$
1980	1998	1422	1974.2	1990	14178.1	1417.9	$(H_2)RhH_2$
	1441			1438			
1920.6	1920.6		1935.5	1936			RhH
	1379.9	1379.9		1390	1389.7		RhD
1606		1169	1608	1612	1172	1165.5	$(H_2)RhH_2^-$
				1236			
1344.6		977.7	1357.2	1433.3	987.7	982.3	$(RhH)_2$
			803.0		574.8	573.0	$(RhH)_2$
737.3			737.6	630.3	565.2		$(H_2)Rh(H_2)$
			706.4		551.9	551.5	aggregate
			677.7		533.9	531.9	aggregate

[a] Associated bands also at 1507.9 and 1497.9 cm^{-1}.

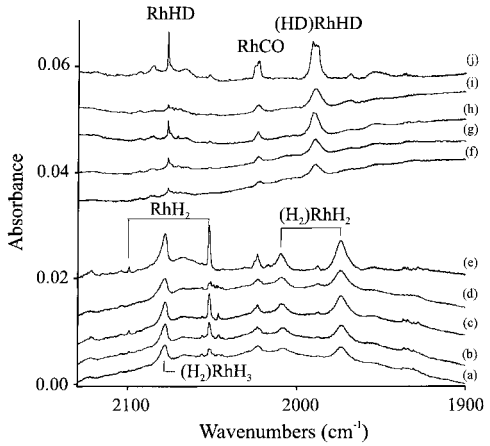

Figure 4. Infrared spectra of laser-ablated rhodium, H_2, and HD reaction products in solid neon: (a) 2% H_2 in neon co-deposited for 60 min at 3.5 K, (b) after annealing to 7 K, (c) after annealing to 9 K, (d) after broadband photolysis, (e) after annealing to 11 K, (f) 2% HD in neon co-deposited for 60 min at 3.5 K, (g) after annealing to 7 K, (h) after broadband photolysis, (i) after annealing to 9 K, and (j) after annealing to 12 K.

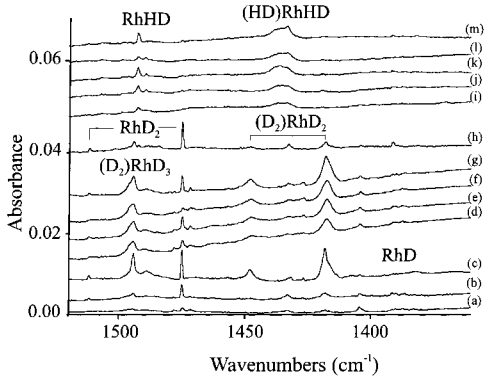

Figure 5. Infrared spectra of laser-ablated rhodium, D_2, and HD reaction products in solid neon: (a) 0.4% D_2 in neon co-deposited for 60 min at 3.5 K, (b) after annealing to 10 K, (c) after annealing to 13 K, (d) 2% D_2 in neon co-deposited for 60 min at 3.5 K, (e) after annealing to 7 K, (f) after broadband photolysis, (g) after annealing to 9 K, (h) after annealing to 13 K, (i) 2% HD in neon co-deposited for 60 min, (j) after annealing for 7 K, (k) after annealing to 9 K, (l) after broadband photolysis, and (m) after annealing to 12 K.

assignment of this band to the diatomic molecule RhH. The absorptions are in good agreement with the fundamentals deduced from gas-phase fluorescence spectra at 1948 ± 18 cm^{-1} for RhH and 1386 ± 14 cm^{-1} for RhD, respectively.[7] The results of DFT calculations for RhH are summarized in Table 2. The BPW91 functional calculations with the SDD pseudopotential are in very good agreement with the gas phase value (only under estimated by 3.6%). However, the LANL2DZ pseudopotential at the same level gives higher frequencies (over estimated by more than 5%). For comparison, higher level calculations give 2054 and 2063 cm^{-1} harmonic frequencies for RhH.[8,10] Note that the calculated frequency of 2031.8 cm^{-1} at the B3LYP/6-311+G(d,p)/LANL2DZ level is 111.2 cm^{-1} high, but using the larger 6-311+G(3df,3pd) basis set gives 1998.7 cm^{-1}, which approaches the observed value satisfactorily, but the SDD pseudopotential gives frequencies that are way too low. It is obvious that the calculated frequencies for rhodium hydrides using DFT are sensitive to the basis set incompleteness.[36]

The 2053.4 cm^{-1} band appeared on deposition, increased 5 times on annealing to 30 K, almost disappeared on broadband photolysis, but appeared again on further annealing in argon (Figure 1). This band undergoes a large shift to 1475.2 cm^{-1} upon reaction with D_2 and defines a 1.3919 H/D isotopic frequency ratio. An experiment with $H_2 + D_2$ gave the same bands. Similar experiments with HD gave two new bands 2077.9 and 1492.9 cm^{-1} with the same 1.3919 H/D ratio, which are 1.2% higher than the above RhH_2 and RhD_2 bands and show evidence of slight coupling between Rh−H vibrations in this molecule. If the 2053.4 cm^{-1} band is due to ν_3 of RhH_2, then the ν_1 vibrational mode is expected another 1.2% higher, and the very weak 2099.4 cm^{-1} band is appropriate. Likewise, if the 1475.2

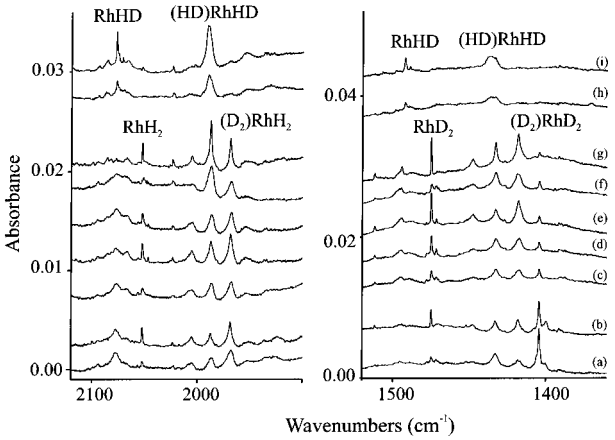

Figure 6. Infrared spectra of laser-ablated rhodium, $H_2 + D_2$, and HD reaction products in solid neon: (a) 4.5% $H_2 + 1.5\%$ D_2 in neon co-deposited at 3.5 K, (b) after annealing to 11 K, (c) 1.5% $H_2 + 1.5\%$ D_2 in neon co-deposited at 3.5 K, (d) after annealing to 7 K, (e) after annealing to 9 K, (f) after broadband photolysis, (g) after annealing to 12 K, (h) 2% HD in neon co-deposited at 3.5 K, and (i) after annealing to 9 K.

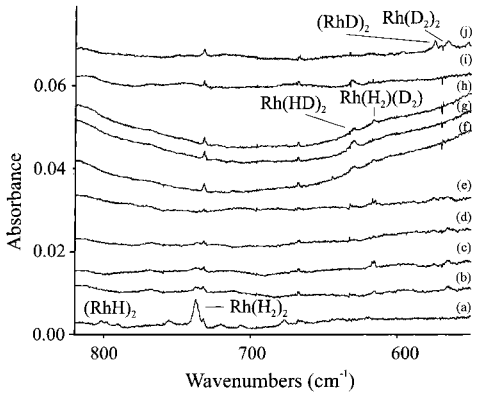

Figure 7. Infrared spectra of laser-ablated rhodium, H_2, $H_2 + D_2$, HD, and D_2 reaction products in solid neon: (a) 2% H_2 co-deposited at 3.5 K, (b) 1.5% $H_2 + 1.5\%$ D_2 co-deposited at 3.5 K, (c) after annealing to 9 K, (d) after photolysis, (e) after annealing to 12 K, (f) 2% HD co-deposited at 3.5 K, (g) after annealing to 9 K, (h) after photolysis, (i) after annealing to 12 K, and (j) 2% D_2 co-deposited at 3.5 K.

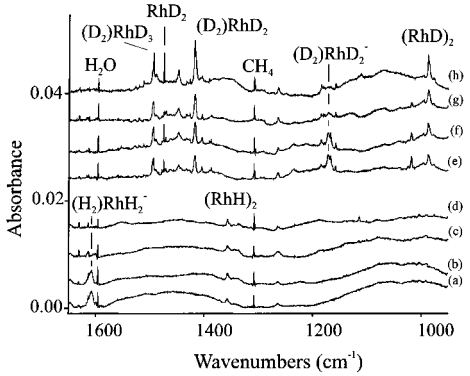

Figure 8. Infrared spectra of laser-ablated rhodium, H_2, and D_2 reaction products in solid neon: (a) 2% H_2 in neon co-deposited at 3.5 K, (b) after annealing to 9 K, (c) after photolysis, (d) after annealing to 12 K, (e) 2% D_2 in neon co-deposited at 3.5 K, (f) after annealing to 9 K, (g) after photolysis, and (h) after annealing to 12 K.

cm^{-1} band is due to ν_3 of RhD_2, then the ν_1 mode should fall another 1.2% higher, and the weak 1512.2 cm^{-1} band fits.

DFT calculations (Table 2) predict an acutely bent (83 ± 1°) RhH_2 $^2A_1$ ground-state molecule, in agreement with higher

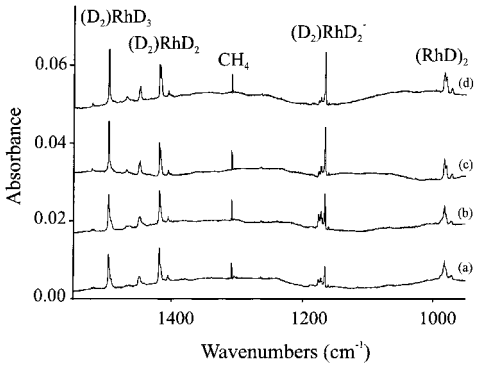

Figure 9. Infrared spectra of laser-ablated rhodium and pure deuterium reaction products: (a) Rh and pure deuterium co-deposited at 3.5 K for 25 min, (b) after photolysis, (c) after annealing to 7 K, and (d) after annealing to 8 K.

TABLE 2: Structures and Frequencies Calculated at BPW91 and B3LYP Levels for RhH and RhH_2

molecule	state	geometry (Å, degree)	frequency, cm^{-1} (intensity, km/mol)
		BPW91/6-311+G(d,p)/LANL2DZ	
RhH	$^3\Delta$	RhH, 1.545	2088.8(174)
RhH_2	$^2A_1$	RhH, 1.529; HRhH, 82.1	2234.7(47), 2163.5(117)
		BPW91/6-311+G(3df,3pd)/LANL2DZ	
RhH	$^3\Delta$	RhH, 1.551	2058.8(123)
RhH_2	$^2A_1$	RhH, 1.532; HRhH, 82.7	2198.9(23), 2146.0(97)
		BPW91/6-311+G(d,p)/SDD	
RhH	$^3\Delta$	RhH, 1.605	1881.2(118)
RhH_2	$^2A_1$	RhH, 1.531; HRhH, 83.5	2206.7(17), 2156.0(77)
		BPW91/6-311+G(3df,3pd)/SDD	
RhH	$^3\Delta$	RhH, 1.602	1877.7(115)
RhH_2	$^2A_1$	RhH, 1.529; HRhH, 83.5	2205.8(16), 2153.9(75)
		B3LYP/6-311+G(d,p)/LANL2DZ	
RhH	$^3\Delta$	RhH, 1.556	2031.8(265)
RhH_2	$^2A_1$	RhH, 1.532; HRhH, 82.5	2230.5(64), 2146.4(193)
		B3LYP/6-311+G(3df,3pd)/LANL2DZ	
RhH	$^3\Delta$	RhH, 1.561	1998.7(205)
RhH_2	$^2A_1$	RhH, 1.533; HRhH, 83.3	2199.8(37), 2129.9(166)
		B3LYP/6-311+G(d,p)/SDD	
RhH	$^3\Delta$	RhH, 1.620	1822.3(175)
RhH_2	$^2A_1$	RhH, 1.533; HRhH, 83.8	2204.2(33), 2135.6(140)
		B3LYP/6-311+G(3df,3pd)/SDD	
RhH	$^3\Delta$	RhH, 1.617	1817.3(172)
RhH_2	$^2A_1$	RhH, 1.530; HRhH, 84.0	2202.7(31), 2132.4(137)

level calculations,[3] and a stronger antisymmetric stretching mode lower by about 50 cm^{-1} than the symmetric stretching mode. The large basis set calculations are in very good agreement: both modes are high by about 100 cm^{-1}, the same error found for RhH. The calculated stretching vibrations of RhH_2 at 2199.8 and 2129.9 cm^{-1} using the B3LYP functional with LanL2DZ/6-311+G(3df,3pd) are slightly lower than BPW91 values and 4.8 and 3.8% higher than observed values.

These assignments to RhH_2 are further substantiated by the neon matrix observations of sharp bands at 2099.7 and 2052.2 cm^{-1} with 1.3887 and 1.3913 H/D frequency ratios and by their 4× growth on annealing, demise on photolysis, and restoration on further annealing (Figure 4). Sharp new 2076.9 and 1492.5 cm^{-1} absorptions with 1.3916 ratio using HD, that are intermediate between the symmetric and antisymmetric stretching modes of RhH_2 and RhD_2, are clearly due to RhHD and confirm this assignment. In fact, the 2076.9 cm^{-1} band is 1.0 cm^{-1} above the average RhD_2 mode, and the 1492.5 cm^{-1} band is 0.9 cm^{-1} below the average RhD_2 mode, which shows a small interaction between the Rh−H and Rh−D stretching modes in RhHD.

TABLE 3: Structures and Frequencies Calculated at the BPW91/6-311++G(d,p)/SDD Level for Other Rh_xH_y Species

species	state	structure (Å, deg)	frequencies, cm^{-1} (intensities, km/mol)
RhH_2 (C_{2v})	$^2A_1$	1.531, 83.5	2206.7 (18), 2155.9 (78), 719.5 (6)
$(H_2)RhH$ (C_{2v})	$^3A_1$	1.832, 0.824 1.595, 167.0	3262.7 (168), 1973.1 (144), 1382.4 (4), 860.5 (19), 672.5 (7), 632.1(3)
RhH_3 (C_{3v})	$^1A_1$[a]	1.520, 83.9	2288.9 (1), 2233.0 (39 × 2), 727.8 (3), 703.4 (1 × 2)
$(H_2)Rh(H_2)$	$^2A'$[b]	1.712, 0.876 1.713., 0.875 159.19, 159.15	2733.3 (38), 2719.4 (161), 1625.0 (4), 1624.9 (4), 1258.9 (0), 756.9 (0), 722.6 (614), 427.3 (3), 426.9 (3)
$(H_2)RhH_2$	^2A[c]	1.573, 1.535, 77.9, 1.794, 1.854, 0.829, 77.9, 158.5, 106.7	3215.3 (195), 2183.2 (26), 2055.1 (130), 1432.4 (24), 865.9 (6), 694.2 (47), ..., 183.0 (3)
$(H)_2RhH_3$	$^1A'$	1.791, 1.856, 0.827 1.564, 1.522, 1.520 158.4, 102.0, 79.4, 83.6	3237.0 (179), 2282.0 (5), 2241.7 (28), 2120.6 (92)
$(RhH)_2$ (D_{2h})	$^3B_{1u}$	1.711, 100.2, 79.8	1544.8 (0), 1402.7 (92), 842.2 (63), 820.9 (0), 350.1 (21), 227.9 (0)

[a] The $^1A_1$ state is 27.3 kcal/mol lower than $^3A_1$ at this level of theory. [b] The same calculation with LANL2DZ gave almost the same structure with 1.724 and 0.864 Å bond lengths and strong 692.6 cm^{-1} absorption; B3LYP/LANL2DZ gave 1.747 and 0.832 Å and 849.0 cm^{-1}; MP2/LANL2DZ gave 1.713 and 0.832 Å and 660.3 cm^{-1}. [c] The ^2A structure is 8.8 kcal/mol lower than $^2A'$ at this level of theory.

TABLE 4: Structure and Frequencies Calculated at the BPW91/6-311++G(d,p)/SDD Level for RhH_x^- Anions (x = 1−4)[a]

anion	state	structure (Å, deg)	frequencies, cm^{-1} (intensities, km/mol)
RhH^-	$^2\Delta$	1.549	2024.4 (101)
RhH_2^- (C_{2v})	$^1A_1$	1.539, 87.1	2128.0 (150), 2092.8 (80), 672.3 (0)
RhH_3^- (C_{2v})	$^2A'$	1.630, 130.2, 1.530, 88.3	2171.3 (111), 1785.1 (182), 1612.2 (332), 560.4 (26), 544.0 (34), 334.3 (187)
RhH_4^- (C_{2v})	$^1A_1$[b]	1.524, 85.0, 1.693, 177.8	2194.5 (131), 1430.2 (1837)
$(H_2)RhH_2^-$	$^1A'$	1.656, 1.005, 1.532, 1.665, 84.4, 161.9, 91.6	2156.4 (129), 2057.9 (129), 1857.4 (22), 1738.1 (231), 734.5 (33), 652.8 (5), 581.1 (19), 533.6 (6), 445.8 (29)

[a] These RhH_x^- (x = 1, 2, and 3) anions are more stable than the corresponding neutrals by 37.1, 22.7, 11.0 kcal/mol, respectively. [b] The $^1A_1$ state is 2.0 kcal/mol less stable than the $^1A'$ state $(H_2)RhH_2^-$, which is 35.4 kcal/mol more stable than the ^2A neutral $(H_2)RhH_2$ species.

In addition to RhH_2, several other RhH_2-like absorptions appear in the 2000 cm^{-1} region. A band at 2036.1 cm^{-1}, just below RhH_2 at 2053.4 cm^{-1} in solid argon, decreases on annealing, but increases on photolysis, and exhibits an H/D frequency ratio, 1.3916, that is almost the same as RhH_2. A sharp band appears at 2046.6 cm^{-1} on annealing in neon, disappears on photolysis along with the 2052.2 cm^{-1} RhH_2 band, and displays a 1.3905 H/D ratio. These bands exhibit no H_2 concentration dependence relative to RhH_2 and are probably due to different argon and neon matrix packing configurations or "sites" for RhH_2 in the matrix cage.

In solid neon, RhH gives a weak, broad 1936 cm^{-1} band on deposition, which sharpens to 1935.5 cm^{-1} on annealing. This feature is within experimental error of the gas-phase fundamental[7] and blue-shifted 14.9 cm^{-1} from the argon matrix value. In contrast, the RhH_2 fundamentals are blue-shifted 0.2 and red-shifted 1.3 cm^{-1} in neon. The yield of RhH is much smaller in solid neon than argon owing to further reaction with hydrogen before solidification. Neither RhD nor RhD_2 are observed in pure solid deuterium as these metal hydrides readily form complexes with D_2.

$Rh(H_2)_2$. The 737.6 cm^{-1} neon matrix absorption increases on annealing, decreases on photolysis, and increases on subsequent annealing, but these changes are small. The band shifts to 630.2 cm^{-1} with HD and to 565.2 cm^{-1} with D_2. Experiments with H_2 and D_2 mixtures gave the 737.6 and 565.2 cm^{-1} bands plus a new stronger absorption at 616.5 cm^{-1} as shown in Figure 7. Note that the 616.5 cm^{-1} band appears at the expense of the 630.2 cm^{-1} absorption on photolysis of the HD sample, and the reverse happens with the $H_2 + D_2$ sample: in each case subsequent annealing partially restores the *original* absorption. Hence, photolysis allows a scrambling of 2HD and of $H_2 + D_2$ and suggests that a $[RhH_4]^*$ excited state is involved. The appearance of a single new mixed isotopic band with $H_2 + D_2$ indicates that two equivalent H_2 molecules are involved in this vibration. The frequency region and H_2/D_2 frequency ratio 737.6/565.2 = 1.305 are both characteristic of side-bound dihydrogen complexes, and $Pd(H_2)_2$, which absorbs at 778.0 cm^{-1}, immediately comes to mind.[6]

BPW91 calculations were done for $Rh(H_2)_2$, and the almost D_{2d} structure is illustrated in Figure 10. The most important characteristic is the strong antisymmetric Rh−H_2 stretching mode computed at 722.6 cm^{-1}, which is very near the observed 737.3 cm^{-1} neon matrix value. Essentially the same structure was calculated with LANL2DZ, with B3LYP, and with MP2, which predicted the strong diagnostic absorption at 692.6, 849.0, and 660.3 cm^{-1}, respectively. These calculations strongly support the identification of $Rh(H_2)_2$ from the matrix infrared spectrum.

A comparison may be made with the similar B3LYP/SDD calculation[6] on $Pd(H_2)_2$: the Rh−H_2 bonds are shorter and H−H bonds longer, which indicate a stronger interaction with Rh than Pd in the bis-dihydrogen complexes.

$(H_2)RhH$. The 2014.0 cm^{-1} band that appears on annealing in solid argon, which traps a large yield of RhH, is assigned to the $(H_2)RhH$ complex (Figure 1). The band shifts to 2013.5 and 1427.6 cm^{-1} with HD and to 1423.7 cm^{-1} with D_2; the 1.4146 H/D frequency ratio is essentially harmonic in contrast to the slight anharmonicity indicated by the 1.3918 ratio for RhH in solid argon.

Support for this assignment is found in our DFT calculations. The $^3A_1$ $(H_2)RhH$ complex is 21.3 kcal/mol more stable than H_2 and $^3\Delta$ ground-state RhH, and the strong Rh−H stretching mode is blueshifted from 1881.1 cm^{-1} for RhH to 1973.1 cm^{-1} for $(H_2)RhH$. The calculated blueshift, 92.0 cm^{-1}, is in excellent agreement with the 93.2 cm^{-1} observed blueshift. Although the $^1A_1$ trihydride RhH_3 is 27.3 kcal/mol more stable than the $^3A_1$ complex $(H_2)RhH$, annealing solid argon to 20−30 K allows

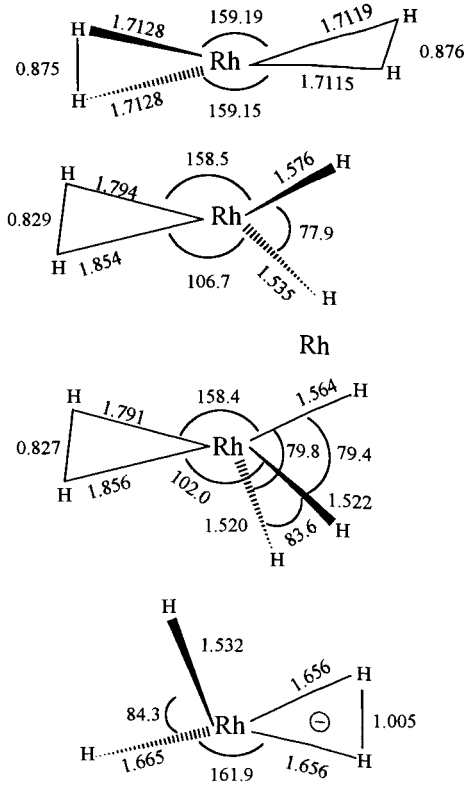

Figure 10. Structures of rhodium hydride dihydrogen complexes calculated at the BPW91/6-311++G(d,p)/SDD level.

only the complex to be formed. Insertion of $^3\Delta$ RhH into H_2 to form RhH_3 probably requires activation energy.

$(H_2)RhH_2$ and $(H_2)RhH_3$. The 2078.2 and 1974.2 cm^{-1} neon matrix bands are favored relative to RhH_2 with increasing H_2 concentration, and the 2078.2 cm^{-1} band is favored slightly more. This is particularly obvious for the deuterium counterparts in pure deuterium (Figure 5) where no isolated RhD and RhD_2 are observed and the upper band set is favored on annealing. In solid neon, the 1974.2 cm^{-1} band increases on annealing, less than RhH_2, whereas the 2078.2 cm^{-1} band does not, and both decrease slightly on broadband photolysis and reproduce on subsequent annealing, but the isolated RhH_2 features do so more dramatically (Figure 4).

The 2078.2 and 1974.2 cm^{-1} bands have spectroscopic properties in common with the sharp 2052.2 cm^{-1} RhH_2 absorption. The 2078.2 cm^{-1} band has a weaker 2122.4 cm^{-1} companion, and the H/D frequency ratios of these bands, 1.3907 and 1.3896, respectively, are extremely close to the ratios for the corresponding 2052.2 and 2099.7 cm^{-1} RhH_2 absorptions, 1.3913 and 1.3887, for symmetric and antisymmetric Rh−H_2 stretching modes. The same is found for the 1974.2 and 2009.4 cm^{-1} bands with 1.3921 and 1.3877 H/D frequency ratios, but notice that the 2009.4 cm^{-1} band is much stronger relative to the 1974.2 cm^{-1} band than the other companion bands. In contrast, the 1974.2 and 2009.4 cm^{-1} absorptions are replaced by a single 1990 cm^{-1} intermediate band with HD, whereas the 2078.2 and 2122.4 cm^{-1} absorptions are replaced by two bands at 2093.6 and 2085.9 cm^{-1}. This means that the lower pair is probably due to coupled Rh−H_2 vibrations, but the upper pair involves a structure that distinguishes between H and D positions. Furthermore, note that calculated frequencies for RhH_3 are higher than those for RhH_2.

Extensive DFT calculations were done for RhH_2 and RhH_3 with side-bonded H_2 in order to model the above absorptions. These approximate calculations support the identification of the higher hydride $(H_2)RhH_{2,3}$ complexes in solid neon and deuterium. Unfortunately, the potential surfaces are relatively flat, and small differences in Rh−H and Rh−H_2 bond lengths make relatively little energy difference. However, the calculations suggest that the addition of an η^2-H_2 ligand to RhH_2 increases one Rh−H band by about 0.04 Å but to RhH_3 decreases two Rh−H bonds by about 0.01 Å. Thus, the bands at 1974.2 and 2009.4 cm^{-1} below RhH_2 (2052.2 and 2099.7 cm^{-1}) are probably due to $(H_2)RhH_2$, and the bands at 2078.2 and 2122.4 cm^{-1} above RhH_2 must be considered for $(H_2)RhH_3$.

On the basis of the experimental observations, the 1974.2 and 2009.4 cm^{-1} bands are assigned to the $(H_2)RhH_2$ complex. The observation of single intermediate bands at 1990 and 1438 cm^{-1} in the Rh−H and Rh-D regions (like for RhH_2) argues that the two Rh−H bonds are more nearly equivalent than predicted by the DFT calculation. A weak, broad band at 2234 cm^{-1} in the deuterium matrix experiment is tentatively assigned to the D−D stretching mode in this species. Further support comes from the mixed $H_2 + D_2$ experiments, which give the pure isotopic product absorptions, new 1987.6 and 1432.9 cm^{-1} absorptions that are near the HD product absorptions and new 2005.3 and 1968.6 cm^{-1} bands just below the H_2 species at 2009.4 and 1974.2 cm^{-1}. The latter bands are assigned to $(D_2)RhH_2$, which is formed on deposition in preference to $(H_2)RhH_2$ as the unreacted H_2 is difficult to condense in solid neon. The 2009.4 and 1974.2 cm^{-1} bands are observed as shoulders in the mixed $H_2 + D_2$ experiments, but annealing favors the 2005.3 and 1968.6 cm^{-1} peaks as more D_2 is trapped than H_2. The 1987.6 and 1432.9 cm^{-1} bands of (HD)RhHD increase on photolysis at the expense of $(D_2)RhH_2$ absorptions; we have no evidence for $(H_2)RhD_2$, which should appear 5−7 cm^{-1} above $(D_2)RhD_2$ as $(D_2)RhH_2$ appears 5.6 cm^{-1} below $(H_2)RhH_2$. The photochemical isotopic redistribution points to a tetrahedral excited state $[RhH_2D_2]^*$ species.

The 2078.2 and 2122.4 cm^{-1} bands are assigned to the $(H_2)RhH_3$ complex because they appear above RhH_2, as RhH_3 is predicted, and the observation of four *new* HD counterpart absorptions requires a distorted RhH_2H' species and rules out C_{3v} symmetry. The DFT calculation provides such a model with two Rh−H stretching frequencies computed above those for RhH_2. Unfortunately, the DFT calculation predicts the unique (longer) Rh−H′ bond stretching mode to be more intense: this absorption is not observed although the region contains other absorptions. On replacement of one H with D, a trigonal MH_2D species retains the strong MH_3 frequency and attains one strong new band in this region,[37] but only new bands are observed here. This species is not observed in solid argon where RhH from the reaction of laser-ablated Rh is trapped, but it is strong in neon and stronger in deuterium where excess $H_2(D_2)$ is available for reaction with excited RhH before condensation. All RhH_3 so formed in excess neon apparently complexes H_2, and all RhD_3 produced with pure deuterium has no choice but to complex D_2 and form $(D_2)RhD_3$. A weak, broad 2272 cm^{-1} band in pure deuterium is tentatively assigned to the D−D stretching mode of this species. We have no evidence for a higher deuteride even in pure deuterium, and DFT calculations find $(H_2)_2RhH_2$ to be much higher in energy than the sum of its parts.

$(H_2)RhH_2^-$. The 1608 cm^{-1} band displays unique properties; it decreases on annealing, disappears on photolysis, and does not return on further annealing. The 1608 cm^{-1} band shifts to 1172 cm^{-1} with D_2, which defines a slightly lower 1.372 H/D frequency ratio. Counterpart bands are observed at 1612 and 1236 cm^{-1} with HD, and $H_2 + D_2$ mixtures gave all of the

above absorptions. This species produced a sharp 1165.5 cm^{-1} band in pure deuterium. A neon experiment with 2% H_2 and 0.2% CCl_4 reduced the 1608 cm^{-1} band to 10% of its former yield with little affect on other product absorptions. Such behavior is characteristic of a molecular anion,[6,27,28] and the 1608 cm^{-1} frequency is substantially lower than the RhH_x absorptions.

Accordingly, DFT calculations were done for RhH_x^- anions to find a strong frequency near 1600 cm^{-1}. The very strong band predicted at 1430 cm^{-1} for RhH_4^- is just too low. In view of the 100 cm^{-1} DFT overestimate for RhH_2, the 1612 cm^{-1} prediction for RhH_3^- is also probably too low, and the failure to observe the second mode near 1785 cm^{-1} helps dismiss the RhH_3^- possiblilty. We must consider $(H_2)RhH_2^-$ with strongest absorption predicted at 1738 cm^{-1} for the longer Rh−H bond, and the 100 cm^{-1} adjustment for RhH_2 brings this calculation into line with the 1608 cm^{-1} band. A weaker 2030 cm^{-1} shoulder with 1463 cm^{-1} deuterium counterpart also tracks with the stronger 1608 and 1172 cm^{-1} absorptions, and they are assigned to the shorter Rh−H bond vibration. The HD product bands at 1612 and 1236 cm^{-1} are due to the (HD)RhH′D$^-$ and (HD)RhD′H$^-$ anion species. In addition, the mixed $H_2 + D_2$ experiments produce the pure isotopic species plus the unique 1236 cm^{-1} (HD)RhD′H$^-$ structure; observation of the HD product shows that a tetrahedral intermediate $[RhH_2D_2]^*$ is involved in the electron capture process as well as the neutral complex.

$(RhH)_2$. The sharp 1357.2 cm^{-1} band increases slightly on annealing, decreases slightly on photolysis, but regenerates on further annealing. The band shifts to 987.7 cm^{-1} with D_2 in neon (1.3741 ratio) and to 982.3 cm^{-1} with pure deuterium. Similar intensity and contour bands at 803.0 and 574.8 cm^{-1} with H_2 and D_2 and a sharp peak at 1433.3 cm^{-1} with HD in neon exhibit the same behavior.

DFT calculations predict a stable $(RhH)_2$ rhombus structure with strong 1402.7 and 842.2 cm^{-1} absorptions, which are in excellent agreement with the observed bands (0.968 and 0.953 scale factors). Again, comparison can be made with palladium: the strongest absorption for $(PdH)_2$ appears at 1347.7 cm^{-1} in solid argon.[6]

Reaction Mechanisms. The endothermic reaction of Rh atoms and H_2 to form RhH, reaction 1, has been performed in the gas phase[7] and in the present matrix-isolation experiments using kinetically energetic[38] laser-ablated Rh atoms:

$$Rh(^4F)^* + H_2 \rightarrow RhH(^3\Delta) + H \qquad \Delta E = 44.0 \text{ kcal/mol}^{39} \quad (1)$$

On the other hand, insertion of ground-state rhodium into H_2 to form $^2A_1$ ground-state RhH_2, reaction 2, is exothermic by 36.0 kcal/mol at the BPW91 level and by 9.5 kcal/mol at the CASSCF level of theory:[3]

$$Rh(^4F) + H_2 \rightarrow RhH_2\,(^2A_1) \qquad \Delta E = -36.0 \text{ kcal/mol} \quad (2)$$

Although theoretical calculations suggested that ground-state $Rh(^4F)$ has a large barrier to insertion but excited $Rh(^2F)$ inserts spontaneously,[3] later calculations show that spin−orbit coupling lowers the barrier for reaction of the atomic ground state.[40] The spectra in Figure 4 demonstrate clearly that reaction 2 proceeds spontaneously in solid neon at 7−9 K, which shows that no significant activation energy is required. The lack of RhHD in the mixed $H_2 + D_2$ experiments further demonstrates that the H + RhH reaction makes no significant contribution to the yield of RhH_2. Rhodium joins platinum[5] as a metal atom that spontaneously inserts into dihydrogen.

The RhH product of reaction 1 has several fates in these experiments. In the more rapidly freezing argon medium, considerable RhH is trapped: on annealing RhH spontaneously forms the $(H_2)RhH$ complex, reaction 3, which apparently requires no activation energy:

$$H_2 + RhH \rightarrow (H_2)RhH \qquad \Delta E = -21.3 \text{ kcal/mol} \quad (3)$$

In the less rapidly freezing neon and deuterium media, RhH dimerizes to $(RhH)_2$, or if sufficiently energetic, RhH* can insert to give RhH_3, which is trapped as $(H_2)RhH_3$.

$$2\,RhH(^3\Delta) \rightarrow (RhH)_2(^3B_{1u}) \qquad \Delta E = -71.5 \text{ kcal/mol} \quad (4)$$

$$H_2 + RhH^* \rightarrow RhH_3(^1A_1) \qquad \Delta E = -48.6 \text{ kcal/mol} \quad (5)$$

$$H_2 + RhH_3 \rightarrow (H_2)RhH_3 \qquad \Delta E = -8.4 \text{ kcal/mol} \quad (6)$$

Likewise RhH_2 also complexes further H_2, and two different structures are produced on co-deposition: the more stable $(H_2)RhH_2$ form increases on annealing, decreases on photolysis, and restores on further annealing, whereas the less stable $Rh(H_2)_2$ structure does likewise to a smaller degree. Furthermore, it is interesting to note that the D_2, H_2, and HD isotopic forms of both species interconvert on photolysis: this shows that a tetrahedral $[RhH_2D_2]^*$ excited state is formed on photoexcitation. Furthermore, $(D_2)RhH_2$ is formed in preference to $(H_2)RhH_2$ in mixed isotopic experiments. (Reaction 3−9 energies computed at BPW91/6-311++G(d,p)/SDD level.)

$$H_2 + RhH_2 \rightarrow Rh(H_2)_2 \qquad \Delta E = -6.0 \text{ kcal/mol} \quad (7)$$

$$H_2 + RhH_2 \rightarrow (H_2)RhH_2 \qquad \Delta E = -8.5 \text{ kcal/mol} \quad (8)$$

$$(H_2)RhH_2 + e^- \rightarrow (H_2)RhH_2^- \qquad \Delta E = -35.4 \text{ kcal/mol} \quad (9)$$

Finally, electrons from the laser-ablation process[27,28] are captured by $(H_2)RhH_2$ to form the molecular anion, which has a substantially lower R−H frequency than the neutral complex. Furthermore, the computed H−H bond length for the anion is significantly longer indicating more reduction of dihydrogen.

Conclusions

Laser-ablated Rh atoms react with H_2 to give RhH_2 and RhH as primary products, which are trapped or react with additional hydrogen in the condensing solid argon, neon, and deuterium matrices. RhH gives a major 1920.6 cm^{-1} band in argon, a minor 1935.5 cm^{-1} band in neon, and no absorption in deuterium owing to further reaction. RhH_2 produces sharp 2099.4 and 2053.4 cm^{-1} and 2099.7 and 2052.2 cm^{-1} bands in solid argon and neon, respectively, and no absorption in deuterium; these absorptions increase on annealing the matrix to allow diffusion, which shows that ground state Rh inserts spontaneously into H_2 and requires little or no activation energy just as was found for platinum.[5] Additional absorptions at 2122.4 and 2078.2 cm^{-1} (1527.3 and 1494.4 cm^{-1} with D_2) in neon and at 1521.1 and 1496.1 cm^{-1} in pure deuterium are assigned to the higher hydride complexes $(H_2)RhH_3$ and $(H_2)RhH_2$, respectively. A weaker 737.6 cm^{-1} absorption in neon is due to the side-bound complex $Rh(H_2)_2$, which is reminiscent of $Pd(H_2)_2$.[6] Both $(H_2)RhH_2$ and $Rh(H_2)_2$ randomize H_2 and D_2 on photolysis. The molecular anion $(H_2)RhH_2^-$ formed on

electron capture also randomizes H and D through a tetrahedral transition state. Rhombic $(RhH)_2$ is observed in all three matrix systems. These assignments are supported by D_2, HD, and $H_2 + D_2$ substitution and density functional theory frequency and structure calculations. DFT calculations work very well to predict the infrared spectra of RhH, RhH_2, $(RhH)_2$, the bis complex, and the $(H_2)RhH_2^-$ anion, but the $(H_2)RhH_{2,3}$ complexes have flat potential surfaces, and minima are difficult to locate. Nevertheless, DFT calculations provide significant useful information.

Acknowledgment. We gratefully acknowledge support from N.S.F. Grant CHE 00-78836.

References and Notes

(1) Parshall, G. W.; Ittel, S. D. *Homogeneous Catalysis*; Wiley-Interscience: New York, 1992.
(2) Wovchko, E. A.; Yates, J. T., Jr. *J. Am. Chem. Soc.* **1995**, *117*, 12557.
(3) Balasubramanian, K.; Liao, D. *J. Phys. Chem.* **1988**, *92*, 6259.
(4) Van Zee, R. J.; Li, S.; Hamrick, Y. M.; Weltner, W., Jr. *J. Chem. Phys.* **1992**, *97*, 8123.
(5) Andrews, L.; Wang, X.; Manceron, L. *J. Chem. Phys.* **2001**, *114*, 1559.
(6) (a) Andrews, L.; Manceron, L.; Alikhani, M. E.; Wang, X. *J. Am. Chem. Soc.* **2000**, *122*, 11011. (b) Andrews, L.; Wang, X.; Alikhani, M. E.; Manceron, L. *J. Phys. Chem. A* **2001**, *105*, 3052.
(7) Balfour, W. J.; Cao, J.; Qian, C. X. W. *J. Mol. Spectrosc.* **2000**, *201*, 244.
(8) Langhoff, S. R.; Pettersson, L. G. M.; Bauschlicher, C. W.; Partridge, H. *J. Chem. Phys.* **1987**, *86*, 268.
(9) Balasubramanian, K.; Liao, D.-W. *J. Chem. Phys.* **1988**, *88*, 317.
(10) Illas, F.; Rubio, J.; Cañellas, J.; Ricart, J. M. *J. Chem. Phys.* **1990**, *93*, 2603.
(11) Mains, G. J.; White, J. M. *J. Phys. Chem.* **1991**, *95*, 112.
(12) Wey, J. P.; Neely, W. C.; Worley, S. D. *J. Phys. Chem.* **1991**, *95*, 8881.
(13) Pei, Z.; Fang, T. H.; Worley, S. D. *J. Phys. Chem.* **1995**, *99*, 3663.
(14) Osborn, J. A.; Jardine, F. H.; Young, J. F.; Wilkinson, G. *J. Chem. Soc. A* **1966**, 1711.
(15) Dewhirst, K. C.; Keim, W.; Reilly, C. A. *Inorg. Chem.* **1968**, *7*, 546.
(16) Ito, T.; Kitazume, S.; Yamamoto, A.; Ikeda, S. *J. Am. Chem. Soc.* **1970**, *92*, 3011.
(17) Bernard, M.; Guiral, V.; Delbecq, F.; Fache, F.; Sautet, P.; Lemaire, M. *J. Am. Chem. Soc.* **1998**, *120*, 1441.
(18) Guiral, V.; Delbecq, F.; Sautet, P. *Organometallics* **2000**, *19*, 1589.
(19) Xiao, Z. L.; Hauge, R. H.; Margrave, J. L. *J. Chem. Phys.* **1991**, *95*, 2696.
(20) Chertihin, G. V.; Andrews, L. *J. Am. Chem. Soc.* **1994**, *116*, 8322.
(21) Chertihin, G. V.; Andrews, L. *J. Am. Chem. Soc.* **1995**, *117*, 6402.
(22) Chertihin, G. V.; Andrews, L. *J. Phys. Chem.* **1995**, *99*, 15004.
(23) Van Zee, R. J.; Li, S.; Weltner, W., Jr. *J. Chem. Phys.* **1995**, *102*, 4367.
(24) Bayse, C. A.; Hall, M. B. *J. Am. Chem. Soc.* **1999**, *121*, 1348.
(25) Burkholder, T. R.; Andrews, L. *J. Chem. Phys.* **1991**, *95*, 8697.
(26) Hassanzadeh, P.; Andrews, L. *J. Phys. Chem. A* **1992**, *96*, 9177.
(27) Zhou, M. F.; Andrews, L. *J. Phys. Chem. A* **1999**, *103*, 7773.
(28) Liang, B.; Zhou, M. F.; Andrews, L. *J. Phys. Chem. A* **2000**, *104*, 3905 and references therein.
(29) Frisch, M. J.; Trucks, G. W.; Schlegel, H. B.; Scuseria, G. E.; Robb, M. A.; Cheeseman, J. R.; Zakrzewski, V. G.; Montgomery, J. A., Jr.; Stratmann, R. E.; Burant, J. C.; Dapprich, S.; Millam, J. M.; Daniels, A. D.; Kudin, K. N.; Strain, M. C.; Farkas, O.; Tomasi, J.; Barone, V.; Cossi, M.; Cammi, R.; Mennucci, B.; Pomelli, C.; Adamo, C.; Clifford, S.; Ochterski, J.; Petersson, G. A.; Ayala, P. Y.; Cui, Q.; Morokuma, K.; Malick, D. K.; Rabuck, A. D.; Raghavachari, K.; Foresman, J. B.; Cioslowski, J.; Ortiz, J. V.; Baboul, A. G.; Stefanov, B. B.; Liu, G.; Liashenko, A.; Piskorz, P.; Komaromi, I.; Gomperts, R.; Martin, R. L.; Fox, D. J.; Keith, T.; Al-Laham, M. A.; Peng, C. Y.; Nanayakkara, A.; Gonzalez, C.; Challacombe, M.; Gill, P. M. W.; Johnson, B.; Chen, W.; Wong, M. W.; Andres, J. L.; Gonzalez, C.; Head-Gordon, M.; Replogle, E. S. and Pople, J. A. *Gaussian 98*, revision A.7; Gaussian, Inc.: Pittsburgh, PA, 1998.
(30) (a) Becke, A. D. *J. Chem. Phys.* **1993**, *98*, 5648. (b) Lee, C.; Yang, W.; Parr, R. G. *Phys. Rev. B* **1988**, *37*, 785.
(31) (a) Becke, A. D. *Phys. Rev. A* **1988**, *38*, 3098. (b) Perdew, J. P.; Wang, Y. *Phys. Rev. B* **1992**, *45*, 13244.
(32) (a) Krishnan, R.; Binkley, J. S.; Seeger, R.; Pople, J. A. *J. Chem. Phys.* **1980**, *72*, 650. (b) Frisch, M. J.; Pople, J. A.; Binkley, J. S. *J. Chem. Phys.* **1984**, *80*, 3265.
(33) (a) Wadt, W. R.; Hay, P. J. *J. Chem. Phys.* **1985**, *82*, 284. (b) Hay, P. J.; Wadt, W. R. *J. Chem. Phys.* **1985**, *82*, 299.
(34) Andrae, D.; Haussermann, U.; Dolg, M.; Stoll, H.; Preuss, H. *Theor. Chim. Acta* **1990**, *77*, 123.
(35) Milligan, D. E.; Jacox, M. E. *J. Mol. Spectrosc.* **1973**, *46*, 460. Wight, C. A.; Ault, B. S.; Andrews, L. *J. Chem. Phys.* **1976**, *65*, 1244.
(36) Bytheway, I.; Wong, W. *Chem. Phys. Lett.* **1998**, *282*, 219.
(37) Chertihin, G. V.; Andrews, L. *J. Phys. Chem.* **1993**, *97*, 10295.
(38) Kang, H.; Beauchamp, J. L. *J. Phys. Chem.* **1985**, *89*, 3364.
(39) Energy calculations at the BPW91/6-311++G(d,p)/SDD level.
(40) Balusubramanian, K.; Dai, D. *J. Chem. Phys.* **1990**, *93*, 7243.